JOURNAL OF MATERIALS SCIENCE 22 (1987) 3240–3252

Mechanical behaviour in compression loading of 2D-composite materials made of carbon fabrics and a ceramic matrix

J. Y. ROSSIGNOL, J. M. QUENISSET, H. HANNACHE, C. MALLET, R. NASLAIN
Laboratoire de Chimie du Solide du CNRS, Université de Bordeaux, 33405-Talence, France
F. CHRISTIN
Société Européenne de Propulsion, Division Propulsion à Poudres et Composites, 33165-Saint Médard en Jalles, France

2D-carbon–carbon/ceramic composites, made from a 2D-carbon–carbon (2D-C–C) porous preform infiltrated with BN, SiC, TiC or B_4C, are mechanically characterized under compression loading in directions parallel or orthogonal to the carbon fabric layers. Three types of behaviour are observed: non-linear and time dependent behaviour, a quasi-linear domain and a "pseudo-plastic" behaviour related to damaging mechanisms. Under *p*-compression, the variations of the Young modulus as a function of compacity obey a parabolic or linear law depending on whether the material is weakly or highly densified. Under *o*-compression, an exponential law is observed whatever the densification degree. The variations of failure strength compacity follow similar laws. Phenomenological models are given which depict quite well the mechanical behaviours of the composites. Under *o*-compression, failure occurs as the result of damaging mechanisms taking place within the intra-layer ceramic bridges binding the fabric layers together. Under *p*-compression, a transition is observed, from inter-layer delamination to intralayer failure, for a critical compacity of about 0.85 provided the infiltrated ceramic is strong enough (i.e. for SiC and TiC). Such a transition is assumed to also occur for 2D-C–C/B_4C composites. On the contrary, for weak ceramic matrices (e.g. BN), failure in *p*-compression always occurs by delamination. The results suggest that the composite toughness could be increased by an optimization of the composite microstructure.

1. Introduction

Carbon–carbon composite materials, obtained according to either liquid impregnation or chemical vapour infiltration (CVI), or eventually by combining both processes, have demonstrated their usefulness in different applications such as re-entry heat shields, rocket nozzles, disc brakes or prosthetic devices. In order to improve their mechanical properties and oxidation resistance, the carbon matrix has been partially or even totally replaced by other refractory materials. As an example, 2D-carbon–carbon (2D-C–C) porous preforms made of a stack of carbon fabrics consolidated by a small amount of pyrocarbon have been successfully densified according to the CVI technique by SiC, SiC + C, TiC, B_4C or BN [1–8]. The main properties of this new family of so-called ceramic–ceramic composite materials, deriving formally from the carbon–carbon and characterized by a hybrid carbon–ceramic matrix, have been reported in detail elsewhere [9–19].

The aim of the present contribution is to compare the mechanical behaviours in compression loading of the 2D-C–C/ceramic composite materials pointing out the peculiarities of each material (related to the intrinsic properties of each ceramic) as well as emphasizing the common features (mostly due to the occurrence of the same 2D carbon skeleton). This work is limited to compression testing that requires only small samples and a simple experimental procedure, since its aim is a comparative understanding of the mechanical behaviour rather than an evaluation of the characteristics used in structure design.

2. Materials and experimental procedure

The materials were obtained according to a two step CVI procedure. In the first step, a stack of carbon fabrics (ex-PAN fibres) was consolidated by a small amount of pyrocarbon resulting from the pyrolysis of CH_4. At this stage, the 2D-C–C material, which will be referred to as 2D-C–C preform, exhibits a high open porosity V_{p_0} (of the order of 0.30 to 0.60). It is strong enough to be machined into any given shape (e.g. into cylinders, $\phi = 8\,mm$; $h = 16\,mm$ for compression testing). Due to the 2D-character of the material, the samples are machined with their axis parallel or perpendicular to the carbon fabric layers, as schematically shown in Fig. 1.

0022–2461/87 $03.00 + .12

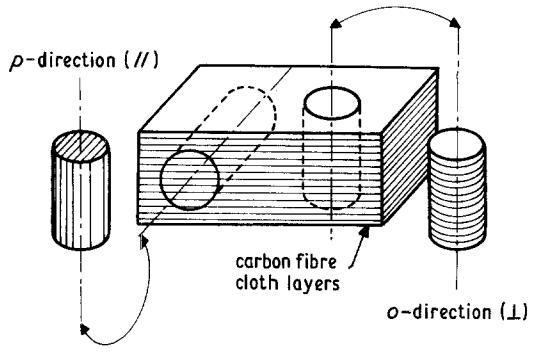

Figure 1 Orientation of the carbon fabric layers within the samples used in the mechanical tests.

In the second step, the porous 2D-C–C preform is progressively densified by a refractory carbide (alone or mixed with pyrocarbon in a few cases) or nitride according to a CVI-technique in a modified LP-CVD apparatus described in detail elsewhere [6–8]. The gaseous precursor is respectively: CH_3SiCl_3–H_2 for SiC; CH_3SiCl_3–Ar for SiC + C; $TiCl_4$–CH_4–H_2 for TiC; BCl_3–CH_4–H_2 for B_4C; BF_3–NH_3 for BN and CH_4 for carbon. As already known for carbon, the CVI-densification of a 2D-C–C preform by a ceramic matrix, in an isotemperature/pressure apparatus, is a rather slow process. The full densification of a preform with V_{p_0} = 0.30 to 0.60 usually requires a CVI-duration greater than one hundred hours. No attempt was made to shorten the CVI-duration by temperature/pressure gradient apparatus [18].

In order to study, for a given material, the evolution of the strength and stiffness as a function of compacity, compression testing was performed on series of samples issued from the same preform and characterized by increasing ceramic volume fraction V_I and thus decreasing residual porosity V_p (or increasing compacity $1 - V_p$) since

$$V_p = V_{p_0} - V_I \quad (1)$$

and

$$1 - V_p = 1 - V_{p_0} + V_I \quad (2)$$

No further machining of the samples was performed after the second CVI-step regarding the hardness and brittleness of the ceramics considered here with respect to the carbon of the 2D-C–C preforms.

In most cases, compression load was applied on the sample at a strain rate of 0.1 mm min^{-1} with a standard equipment.

3. Compression behaviour of 2D-C–C/ceramic composite materials

3.1. Stress–strain relationship

When loaded in compression, the stress–strain relationship of all the 2D-composite materials considered here can be discussed on the basis of four strain domains, as illustrated in Fig. 2 for the initial 2D-C–C preforms and summarized as follows:

(a) In domain I (i.e. for $0 < \varepsilon < \varepsilon^A$), a progressive rigidification of the material corresponding to a delayed elastic behaviour takes place and leads to a non-linear relationship which is particularly apparent for the most porous composite materials.

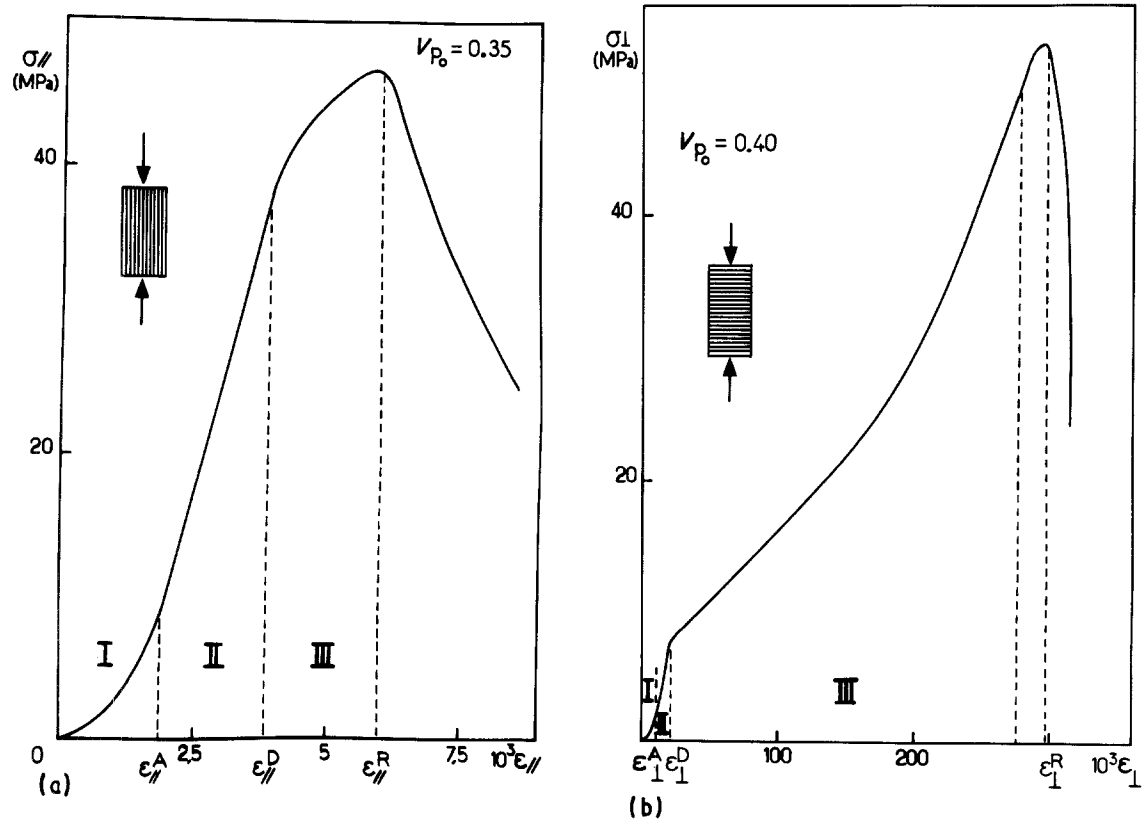

Figure 2 Typical stress–strain curves of 2D-C–C/ceramic composite materials (drawn here for the initial 2D-C–C preforms, i.e. for V_I = 0), when loaded in compression: (a) in *p*-direction, (b) in *o*-direction.

TABLE I Young modulus E, stress and strain at failure (σ^R, ε^R), stress and strain corresponding to the beginning of damaging (σ^D, ε^D) for various 2D-C–C/ceramic composite materials densified by CVI up to the same compacity $1 - V_p = 0.85$

Composite materials	2D-C–C preform V_{p_0}	E(GPa)		σ^R(MPa)		$10^3\ \varepsilon^R$		σ^D(MPa)		$10^3\ \varepsilon^D$	
		∥	⊥	∥	⊥	∥	⊥	∥	⊥	∥	⊥
2D-C–C/BN	0.50–0.60	21	2.5	55	140	7	160	50	40	5	25
2D-C–C		22		100		8					
2D-C–C/SiC + C	0.35	23		110				90		7	
2D-C–C/TiC	0.40–0.45	30	8	150	190	7	80	140	60	6	20
2D-C–C/SiC	0.30	32		180		8		110		6	
2D-C–C/$\overline{B_4C}$	0.40	37	11	190	220	8.5	80	180	150	7	50

(b) In domain II (i.e. for $\varepsilon^A < \varepsilon < \varepsilon^D$), the material is mainly linear elastic. However, it comes out that it is not easy to define accurately ε^A and to derive the compression moduli $E_\parallel$ and $E_\perp$ from the stress–strain curves even after several loading cycles.

(c) In domain III (i.e. for $\varepsilon^D < \varepsilon < \varepsilon^R$), the material is progressively damaged due to matrix microcracking. This important domain is particularly extended in o-compression. On the contrary, it can be sometimes almost non-existent in p-compression.

(d) In domain IV (i.e. for $\varepsilon > \varepsilon^R$), the material collapses mechanically by complete disintegration in o-compression and either by fabric layer buckling or by transverse shearing in p-compression.

Thus, it appears that non linear stress–strain relationship is a significant feature of 2D-C–C/ceramic composite materials whatever the nature of the ceramic matrix.

As shown in Table I and Fig. 3, 2D-C–C/ceramic composite materials densified up to the same level (i.e. $V_p = 0.15$ or $1 - V_p = 0.85$) can be ranked on the basis of both increasing strength and stiffness, despite the fact that the initial preforms did not have exactly the same V_{p_0}. This classification follows, at least roughly the increase in rigidity and brittleness known to occur in the corresponding monolithic ceramics from BN to $\overline{B_4C}$.

3.2. Evolution of the mechanical behaviour as a function of compacity

3.2.1. Influence of compacity $1 - V_p$ on stiffness

The variations of the material rigidities as a function of the compacity $1 - V_p$ achieved after increasing CVI-durations (performed on preforms having roughly the same open porosity V_{p_0}) are shown in Fig. 4. As said above, the highest stiffness is obtained with $\overline{B_4C}$ and the most compliant material corresponds to BN.

In p-direction

–for weakly densified materials (i.e. $1 - V_p < 0.80$), the $E_\parallel = f(1 - V_p)$ relationship is non linear, parabolic curves fitting quite well the experimental data;

–for highly densified materials (i.e. $1 - V_p > 0.80$), $E_\parallel$ increases linearly with $1 - V_p$ according to laws which are formally similar to the so-called mixture law. Thus, the efficiency of the infiltrated ceramic phase on, the material rigidity can be characterized by the slope η of the $E_\parallel = f(1 - V_p)$ straight line for $1 - V_p > 0.80$ (see Table II).

In o-direction

–the evolution of $E_\perp$ as a function of $1 - V_p$ remains non-linear in the whole range of compacity. J. Y. Rossignol *et al.* have already reported such a feature and shown that an exponential law fits quite well the experimental data for 2D-C–C/TiC composite

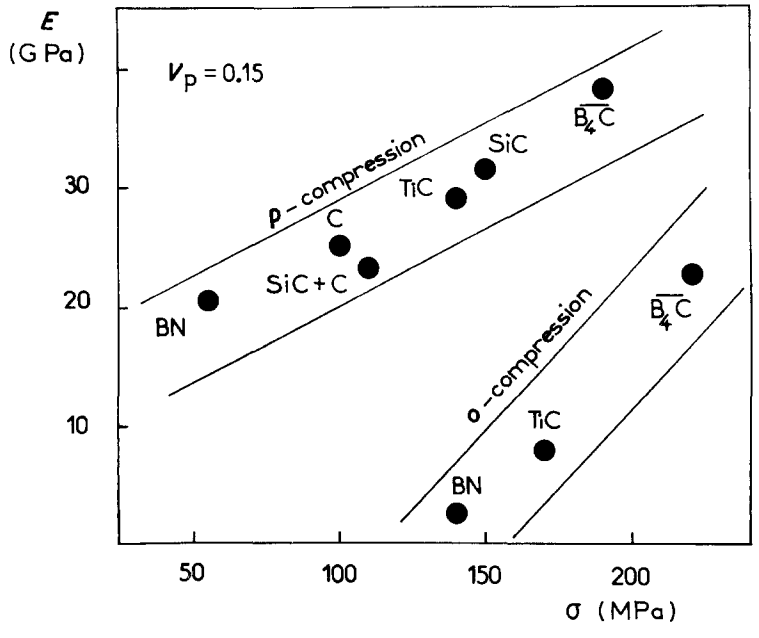

Figure 3 Classification of 2D-C–C/ceramic composites (having the same residual porosity $V_p = 0.15$) on the basis of their Young modulus and rupture strength.

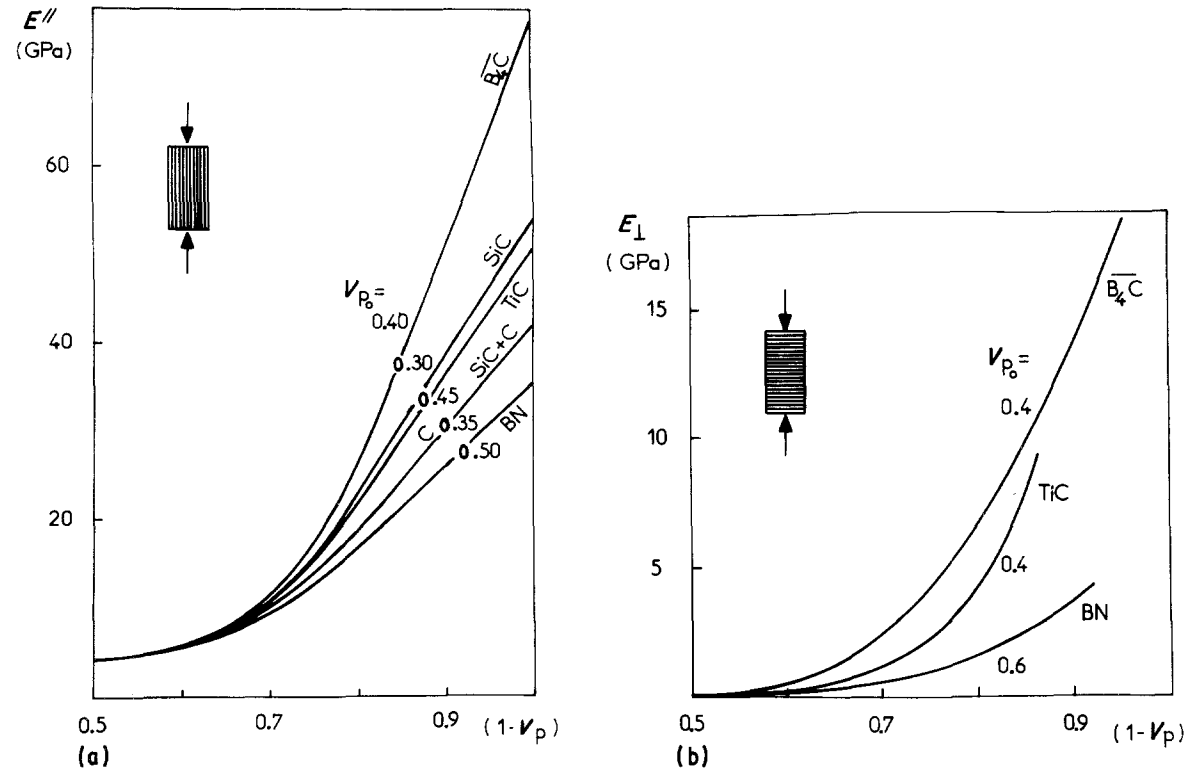

Figure 4 Variations of the Young modulus of 2D-C–C/ceramic composites vs compacity $1 - V_p$ under: (a) *p*-compression loading, (b) under *o*-compression loading.

materials [14, 15]. Such a finding appears to be a common feature for all the related materials, as shown in Fig. 5. Thus, in *o*-compression, the CVI efficiency parameter can be taken as the slope δ of the $L_n E_\perp = f(1 - V_p)$ straight line (see Table II).

3.2.2. Influence of compacity $1 - V_p$ on strength

In *p*-direction

–the main features of the evolution of the rupture strength $\sigma_\parallel^R$ as a function of $1 - V_p$ are very similar to those reported above for rigidity, as shown in Fig. 6. Again, the strength efficiency of the infiltrated ceramic can be characterized by an efficiency parameter ξ taken as the slope of the $\sigma_\parallel^R = f(1 - V_p)$ straight line for $1 - V_p > 0.80$–0.85.

In *o*-compression

–the compression strength has to be described with two characteristics: the rupture strength $\sigma_\perp^R$ and the strength $\sigma_\perp^D$ at which microcracking begins to take place in the material. $\sigma_\perp^R$ which is formally equivalent to the yield strength for a metal, is far lower than $\sigma_\perp^R$ when the composite material is only weakly densified (see Fig. 2b and 6b).

As already mentioned for stiffness, the variations of $\ln \sigma_\perp^R$ and $\ln \sigma_\perp^D$ as a function of $1 - V_p$ are represented by straight lines whose slopes γ and β can be used to characterize the strengthening efficiency of the infiltrated ceramic (Fig. 7 and Table III). It is noteworthy that highly densified 2D-C–C/$\overline{B_4C}$ composite materials are characterized by a relatively low γ value regarding the high compression strength of $\overline{B_4C}$ itself (i.e. about 2800 MPa) (Table IV).

Thus, it appears that $\overline{B_4C}$ results in the best reinforcing effect, on a stiffness and strength point of view, in both *p*- and *o*- directions. However, one has now to study whether the reinforcing effect of $\overline{B_4C}$ is associated or not with an unwished decrease in failure strain ε^R, i.e. with an increase in brittleness (as it could be expected from the somewhat low value of $\gamma_{\overline{B_4C}}$ related to highly densified composites).

3.2.3. Variations of $\varepsilon_\parallel^D$ and $\varepsilon_\parallel^R$ as a function of $1 - V_p$

As shown in Fig. 8, the variations of the strains at yielding $\varepsilon_\parallel^D$ and at rupture $\varepsilon_\parallel^R$ as a function of $1 - V_p$ of materials loaded in *p*-direction, appear quite different depending on the stiffness and brittleness of the infiltrated ceramic phase.

TABLE II Rigidity efficiency parameters η (*p*-compression for $1 - V_p > 0.80$) and δ (*o*-compression) of the CVI infiltrated ceramic for various 2D-C–C/ceramic composite materials (V_{p_0} is the initial open porosity of the 2D-C–C preform)

Infiltrated phase	BN	C	SiC	TiC	SiC	$\overline{B_4C}$
V_{p_0}	0.50		0.35	0.40	0.30	0.40
η(GPa)	90	110	110	140	150	250
δ	8	8		13		18

TABLE III Strength efficiency parameters ξ (*p*-compression for $1 - V > 0.80$–0.85), γ and β (*o*-compression) of the CVI-infiltrated ceramic for various 2D-C–C/ceramic composite materials (V_{p_0} is the initial open porosity of the 2D-C–C preform)

Infiltrated phase	BN	SiC + C	TiC	SiC	$\overline{B_4C}$
V_{p_0}	0.50	0.35	0.40	0.30	0.40
$\xi_{(MPa)}$	200	1200	1300	1400	1500
γ	1.9		3.8		3.4
β	7		8		9

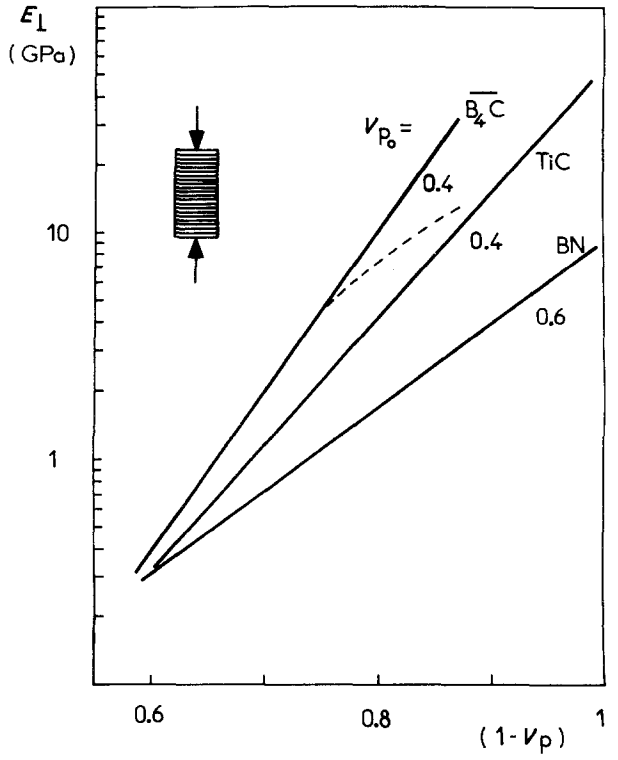

Figure 5 Variations of the Young modulus $E_\perp$ as a function of compacity $1 - V_p$ of 2D-C–C/ceramic composites loaded in *o*-compression, represented in a semi-logarithmic scale.

A slight monotonous decrease of both $\varepsilon_\parallel^D$ and $\varepsilon_\parallel^R$ is observed for 2D-C–C/BN composites. On the other hand, a sharp discontinuity appears in the $\varepsilon_\parallel^D = f(1 - V_p)$ and $\varepsilon_\parallel^R = f(1 - V_p)$ curves for both TiC and $\overline{B_4C}$ based composites. This evolution, corresponding first to an increase in $\varepsilon_\parallel^D$ or $\varepsilon_\parallel^R$ followed by a sharp decrease and to a further increase in strain, is typical of 2D-C–C/TiC composite materials and has been correlated to a failure mode transition [14, 15].

TABLE IV Mechanical properties in compression loading of several CVI ceramics

Ceramic	BN	TiC	βSiC	$\overline{B_4C}$
σ(MPa)	300	750	1035	2860
E(GPa)	88	410	470	490

For 2D-C–C/$\overline{B_4C}$ materials, it is noteworthy that $\varepsilon_\parallel^D$ and $\varepsilon_\parallel^R$ reach high values for partially infiltrated materials (i.e. $1 - V_p \approx 0.8$). Unfortunately, the sharp decrease in strain that occurs for $1 - V_p \approx 0.8$ is apparently not compensated by a further increase in $\varepsilon_\parallel^D$ or $\varepsilon_\parallel^R$ for very high values of compacity (however, fully densified materials have not been studied yet). Thus, 2D-C–C/$\overline{B_4C}$ composites could be more brittle than the related 2D-C–C/TiC or 2D-C–C/SiC materials, unless specific fibre surface treatment is applied (such treatments were not applied to any material in present study).

3.2.4. Variation of the anisotropy in compression properties as a property of $1 - V_p$

The ratio $E_\parallel/E_\perp$, which can be taken to assess the material stiffness anisotropy is quite significant (i.e. > 10) for the initial 2D-C–C preforms (with $1 - V_p \approx 0.6$) as shown in Fig. 9. On the other hand, $\sigma_\parallel^R/\sigma_\perp^R$ is much smaller (i.e. ≈ 0.2 for $1 - V_p \approx 0.6$), compared to one (isotropy). In both cases, increasing $1 - V_p$ by CVI of a ceramic matrix gives rise to a strong decrease in the compression behaviour anisotropy. The evolution towards isotropy is more

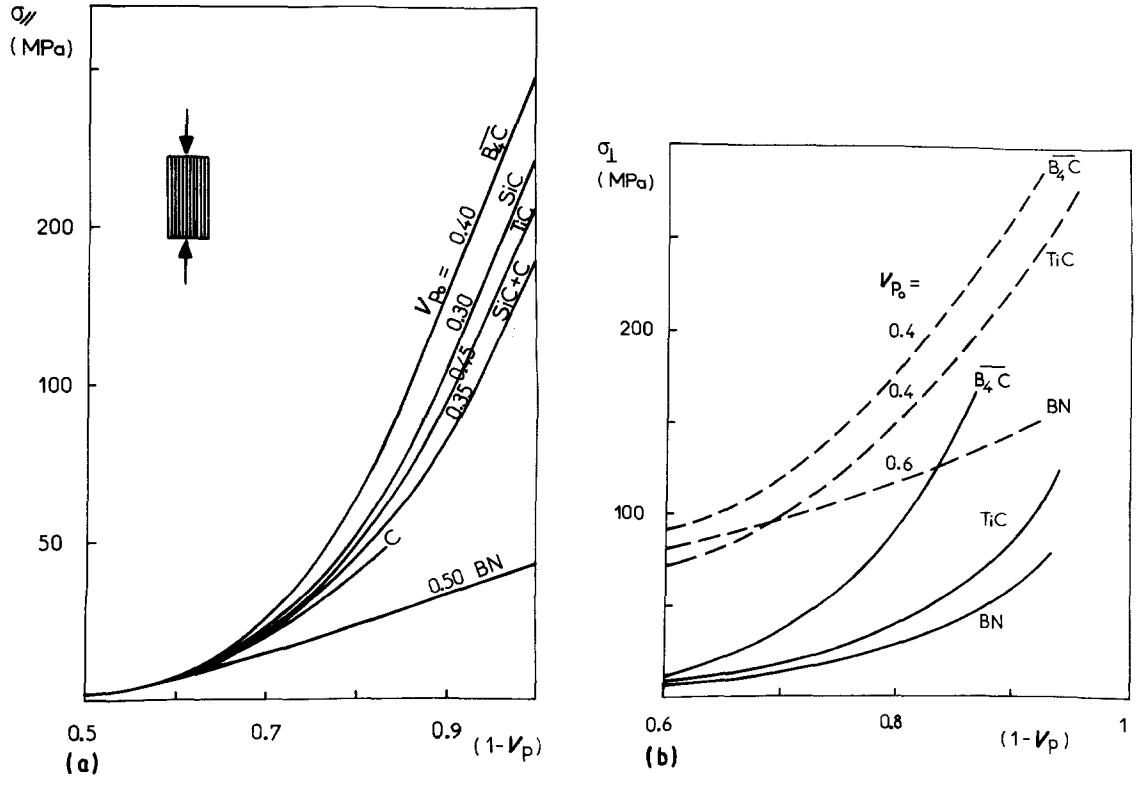

Figure 6 Variations of the strength of 2D-C–C/ceramic composites as a function of compacity $1 - V_p$: (a) rupture strength $\sigma_\parallel^R$ under *p*-compression loading, (b) rupture strength $\sigma_\perp^R$ and damaging strength $\sigma_\perp^D$ under *o*-compression loading. (– – –) $\sigma_\perp^R$, (——) $\sigma_\perp^D$.

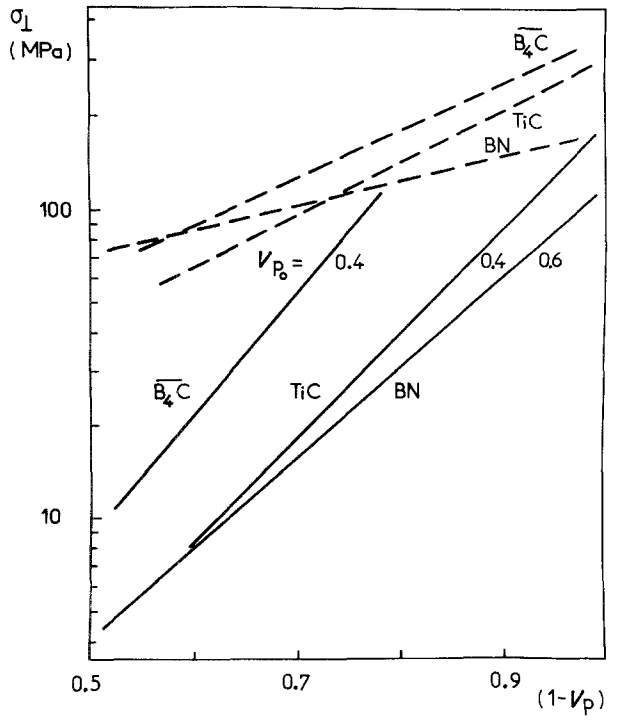

Figure 7 Variations of rupture strength $\sigma_{\perp}^{R}$ and damaging strength $\sigma_{\perp}^{D}$ as a function of compacity $1 - V_p$ for 2D-C–C/ceramic composites loaded in *o*-compression ($\sigma_{\perp}^{R}$ and $\sigma_{\perp}^{D}$ are given in a logarithmic scale).

drastic as the mechanical strength and rigidity of the infiltrated ceramic matrix are higher.

The variations of $\sigma_{\parallel}^{R}/\sigma_{\perp}^{R}$ as a function of $1 - V_p$, for the TiC and $\overline{B_4C}$ based materials, are very similar although the mechanical properties in compression of B_4C and TiC are different (Table IV). This feature has to be related to the anomaly already mentioned for the γ values and to the evolution of $\varepsilon_{\parallel}^{R}$ (or $\varepsilon_{\parallel}^{D}$) as a function of $1 - V_p$. These differences among the infiltrated ceramics are so important that isotropy in rupture strength is already achieved for uncompletely densified 2D-C–C/$\overline{B_4C}$ composites while it is not reached for 2D-C–C/BN composites almost fully densified.

All the data which have been presented in this section support a given hierarchy, on a mechanical point of view, among the 2D-C–C/ceramic composite materials, which corresponds quite well to that already known for the related unreinforced ceramics.

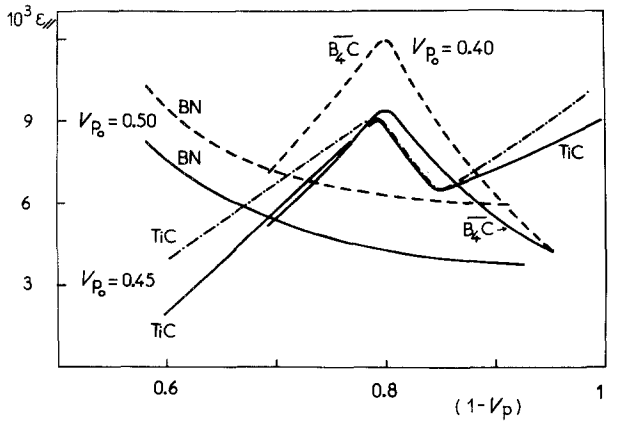

Figure 8 Variations of the compression yield (——) $\varepsilon_{\parallel}^{D}$ and rupture strains (– – –, –·–·–) $\varepsilon_{\parallel}^{R}$ as a function of compacity $1 - V_p$ of 2D-C–C/ceramic composites loaded in *p*-direction.

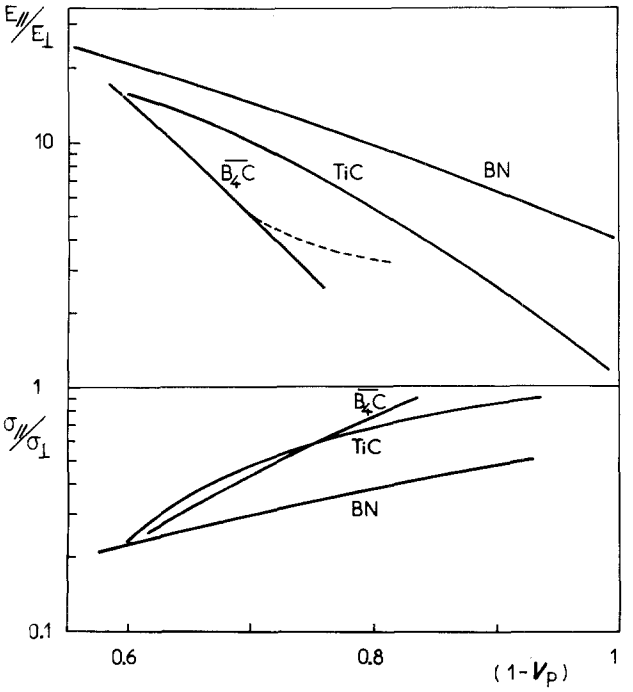

Figure 9 Variations of the anisotropy in the Young modulus and rupture strength of 2D-C–C/ceramic composites loaded in compression as a function of compacity $1 - V_p$.

However, a higher rupture strength could be expected for 2D-C–C/$\overline{B_4C}$ composites from the high compression strength of $\overline{B_4C}$.

4. Discussion

4.1. Non linear elasticity and inelasticity (domain I)

Most 2D-C–C/ceramic composite materials exhibit, in domain I of the stress–strain compression curve, a non-linear behaviour which is significant only for the most porous materials (Fig. 2). This apparent non-linearity can be due to (i) a non-linearity in the testing machine deformation, (ii) geometrical imperfection of the samples or (iii) a non-linear elastic (or eventually inelastic) behaviour of the materials which could lead, for example, to some damping effect.

Since it is difficult to glue strain gauges on the most porous composites without modifying locally the material response, differential methods were used to assess the origin of this non-linear feature as follows:

(a) Experiments were performed in domain I (as well as in the beginning of domain II) on rather large samples of 2D-C–C preforms (25 × 25 × 50 mm; $V_{p_0} = 0.50$) under *o*- and *p*-compression loading. The true testing machine deformation was removed from the experimental curves with a computer (from the record of the compression deformation of a thin steel sheet 25 × 25 × 5 mm^3). The resulting corrected stress–strain curves clearly show evidence of non-linearity which is not related to the testing machine (Fig. 10).

(b) *p*-compression load cycles were successively applied to a 2D-C–C/TiC composite material at increasing stress levels, as illustrated in Fig. 11. The different contributions to the total deformation ε_i^t for each cycle are:

ε_i^e the elastic strain $\varepsilon_i^e = \varepsilon_i^l + \varepsilon_i^n$ due to both testing

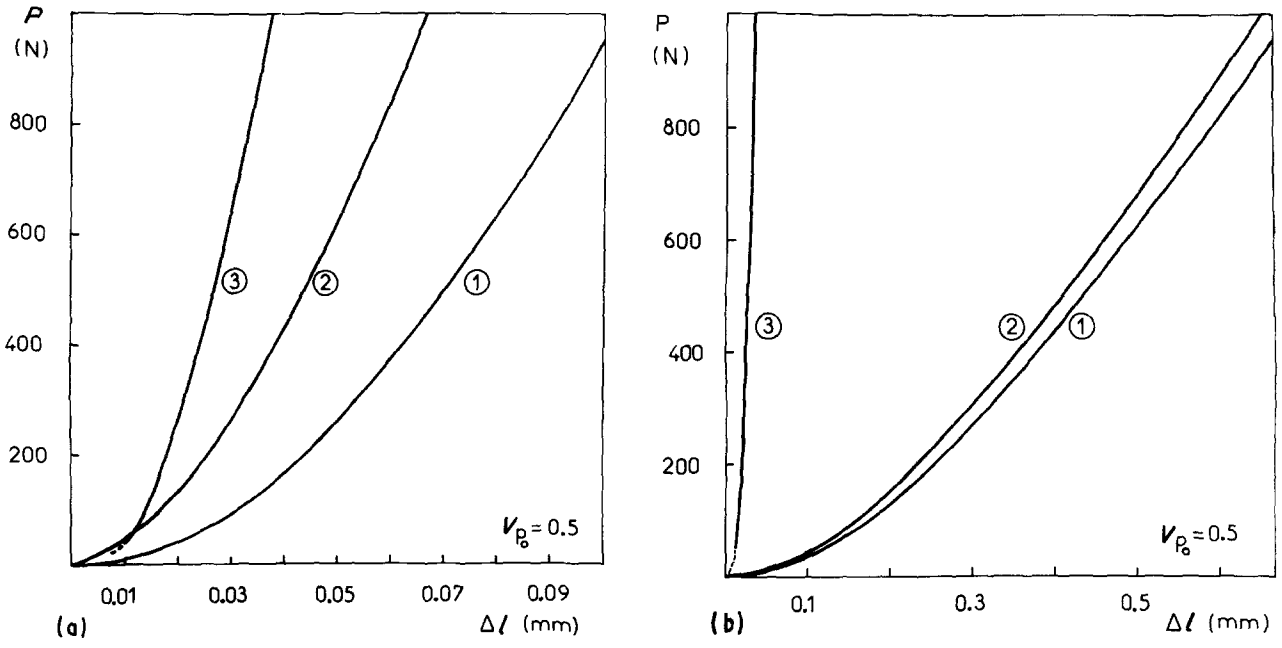

Figure 10 Load-deformation curves of a 2D-C–C preform before (1) or after (2) substraction of the testing machine deformation (3), under (a) *p*-compression, (b) *o*-compression.

machine and sample, ε_i^l and ε_i^n being respectively the linear and non-linear contributions

ε_i^r the residual strain due to sample damaging or delayed elastic strain corresponding to both testing machine and sample,

with

$$\varepsilon_i^t = \varepsilon_i^l + \varepsilon_i^n + \varepsilon_i^r \quad (3)$$

The evolution of the different strains, as the compression load cycles are performed at increasing stress levels, is shown in Fig. 12. The non-monotonous curve corresponding to ε_i^n points out the contribution of the sample in the non-linear elastic strain. This non-linear contribution is indeed significantly reduced when ε_i^r increases, i.e. when the sample begins to be damaged (for $\sigma_{\parallel} > \sigma_{\parallel}^D$).

Therefore, the non-elastic stress–strain relationship found in domain I has, at least partly, to be related to the sample. For example, slightly densified 2D-composite materials could be represented, in a mechanical point of view, by numerous elementary beams finding new fulcrums as load is applied. This representation of the material behaviour at the beginning of compression loading is in agreement with the time dependence of the stress–strain curve since friction can be associated with the relative displacements of all the elementary beams constituting the composite microstructure. This feature of the 2D-composite materials, which is illustrated by the relaxation curve shown in Fig. 13, leads to a non-linear evolution of ε_i^e (Fig. 12). One has to mention that imperfection in the sample geometry could lead to similar behaviour particularly when the loading surfaces are not perfectly parallel (no surface machining was performed after the second CVI-step as said above).

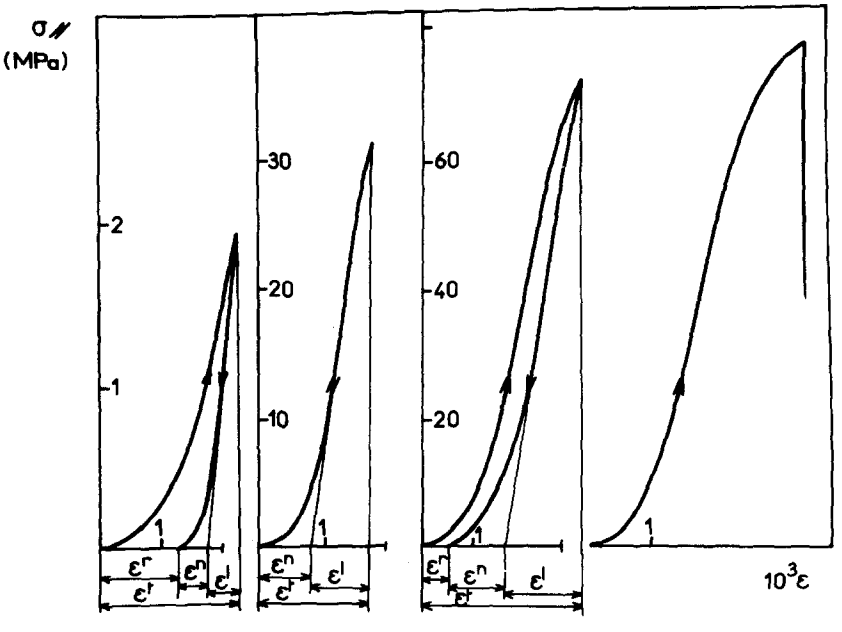

Figure 11 Compression load cycling applied in *p*-direction to 2D-C–C/TiC composites (V_{P_0} = 0.35; V_P = 0.20; V_{TiC} = 0.15) at increasing stress levels.

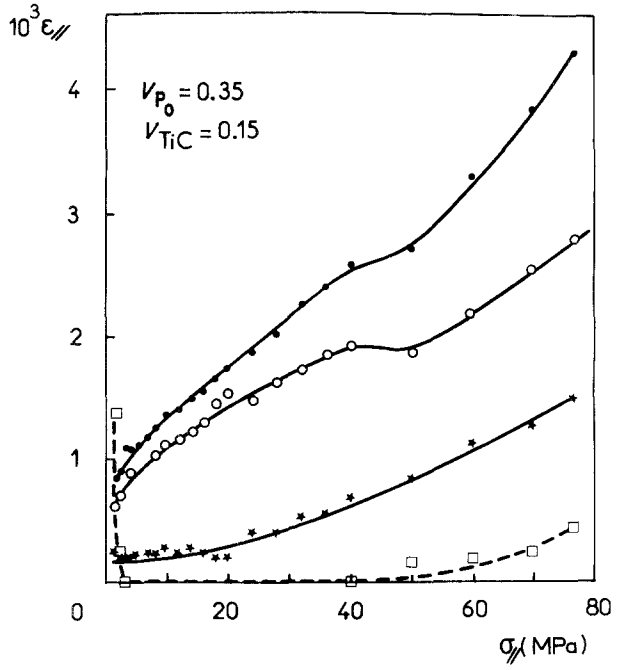

Figure 12 Variations of the strains against stress level for 2D-C–C/TiC composites loaded in *p*-compression. (●) ε^e, (○) ε^n, (★) ε^l, (□) ε^r

(c) Therefore an optical device was used to point out the non-linearity of the stress–strain curve. Actually, the experiments which were performed on large samples did exhibit in domain I a non-linearity which has to be attributed to the material.

Although the influence of the strain rate has not been investigated, the delayed elasticity and energy dissipation (hysteresis loop) in domain I show some similitude with visco-elasticity. On the other hand, the significance of the non-linearity and the time-dependency corresponding to domain I decrease strongly as 2D-C–C/ceramic composite materials are approaching full densification. Nevertheless, the above analysis gives some arguments leading to consider the damping effect has not to be totally excluded of the 2D-composite mechanical behaviour.

4.2. Elastic behaviour (domain II)

As already said, the limit between domains I and II is difficult to assess due to the time dependence of strain. Thus, Young moduli derived from the first loading stress–strain curve are underestimated and must be considered as comparative values. Even more, a detailed analysis of the linear part of the stress–strain curves shows a sigmoidal shape with an inflexion point, i.e. a slight deviation from a true linear elastic behaviour. Some microcracking could be one of the sources of non-linearity (it is quite evident for the materials only slightly infiltrated with a very brittle phase (e.g. TiC or $\overline{B_4C}$) and loaded in *p*-direction).

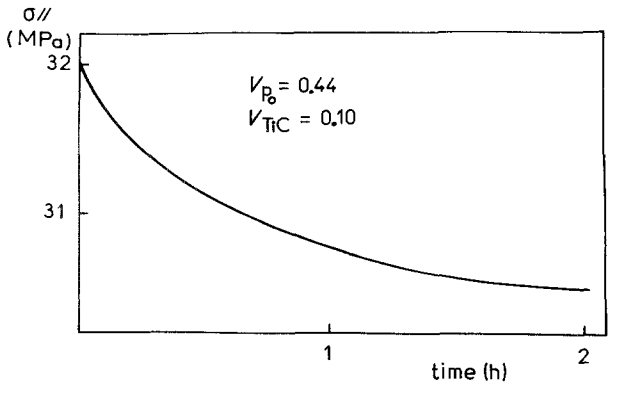

Figure 13 Stress relaxation curve for 2D-C–C/TiC composites loaded in *p*-compression.

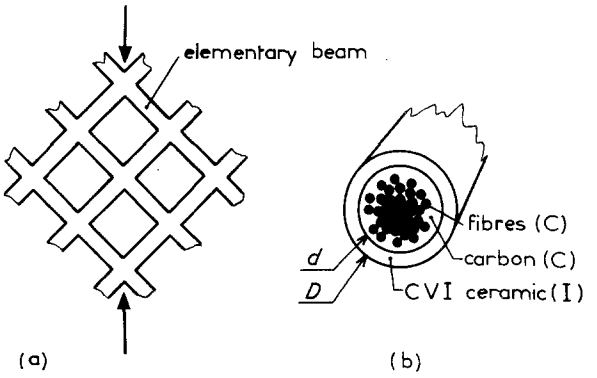

Figure 14 Schematic representation of the layer structure of weakly densified 2D–C–C/ceramic composite materials: (a) association of elementary microstructural beams, (b) cross-section of an elementary beam with a ceramic phase.

4.2.1. Representation of the 2D-C–C/ceramic composite behaviour under *p*-compression

When incompletely densified (i.e. for $V_p > 0.20$), 2D-C–C/ceramic composite materials can be regarded as a structure made of numerous elementary beams which are bending when the material is loaded in *p*-compression, leading to a quasi-linear stress–strain relationship (domain II) as soon as it is stabilized (i.e. for $\varepsilon_{\|} > \varepsilon_{\|}^{A}$) (Fig. 2a and 14a). The elastic strain is indeed mainly controlled by the contraction of the fabric layers. The only role of the interlayer matrix is to prevent fabric layer buckling, as schematically represented in Fig. 15a.

Thus, the compliance of each elementary beam, with respect to bending, can be represented, in a first approximation, by the following equation

$$C \sim L^3/E_B I_B \tag{4}$$

where L, E_B and I_B are respectively the free length, the longitudinal Young modulus and section inertia with respect to bending, of an elementary beam with

$$E_B I_B = E_C I_C + E_I I_I \tag{5}$$

$$I_C = \frac{\pi d^2}{34} \tag{6}$$

and

$$I_I = \pi \frac{D^4 - d^4}{32} \tag{7}$$

where the subscripts C and I refer respectively to the carbon preform and to the ceramics, d and D being defined schematically in Fig. 14b.

Equations 6 and 7 lead to consider I_C and I_I as respectively proportional to V_C^2 and V_I $(V_I + 2V_C)$ where V_C and V_I are the volume fractions of carbon

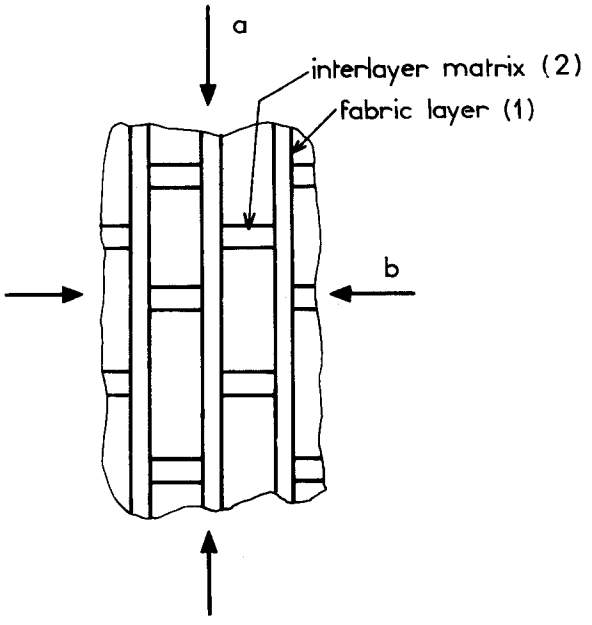

Figure 15 Model for a 2D-C–C/ceramic composite based on a coupling between two phases: (a) in parallel under *p*-compression, (b) in series under *o*-compression.

(fabrics + pyrocarbon) and infiltrated ceramics. Thus, if one assumes that the composite deformation is due to the bending of all the elementary beams, the Young modulus of the composite is given, in a first approximation, by the following equation:

$$E_{\parallel} \sim E_C V_C^2 + E_I V_I^2 + 2E_I V_I V_C \qquad (8)$$

The above model (i.e. Equation 7) has been compared to experimental data by plotting $dE_{\parallel}/dV_I$ as a function of $1 - V_p$ ($V_I + V_C = 1 - V_p$ and $dV_I = d(1 - V_p)$ since V_C = constant for materials deriving from the same 2D-C–C preform), as shown in Fig. 16. The linearity of the ascent part of the curves (for $1 - V_p < 0.8$) observed for either $\overline{B_4C}$, TiC or BN infiltrated ceramics supports the validity of the model, at least for 2D-C–C/ceramic composites incompletely densified. In fact, the model leads to an equation which is no more than an other representation of the rule of mixture.

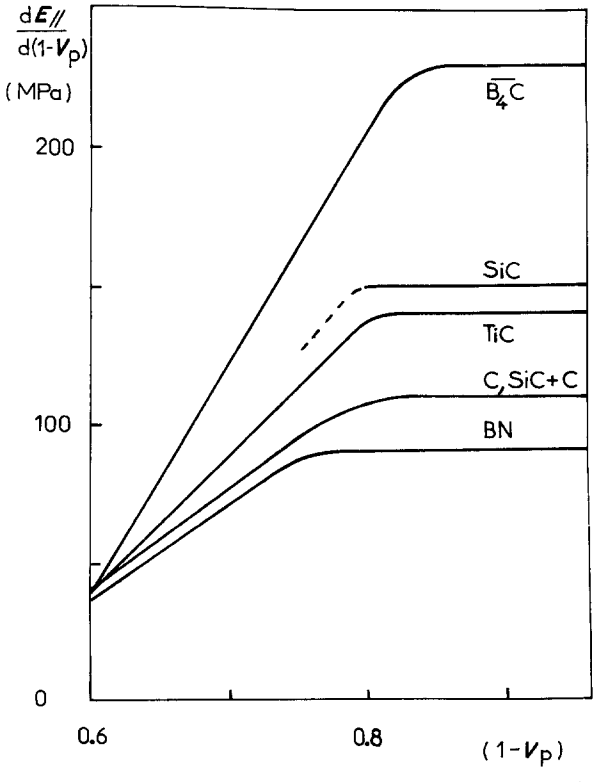

Figure 16 Variations of $dE_{\parallel}/d(1 - V_p)$ as a function of compacity $1 - V_p$ for 2D-C–C/ceramic composites loaded in *p*-compression (data taken from Fig. 4).

On the other hand, for highly densified composites (i.e. for $1 - V_p > 0.80$), the linearity of the $E_{\parallel} = f(1 - V_p)$ curves (see Fig. 4) or the plateaus of the $dE_{\parallel}/dV_I = f(1 - V_p)$ curves (see Fig. 16), lead to consider the materials as an association of three components (namely carbon, infiltrated ceramics and pores) which obeys the rule of mixture under its classical form

$$E_{\parallel} = E_C V_C + E_I V_I \qquad (9)$$

In such a case, the elementary beams cannot be considered any longer as bending elements. The material is rather represented by a porous aggregate of two phases loaded in compression. A similar evolution of $\sigma_{\parallel}^R$ as a function of $1 - V_p$ confirms the two above models (Fig. 6a).

4.2.2. Representation of the 2D-C–C/ceramic composite behaviour under *o*-compression

The above models are more difficult to apply to *o*-compression although bending can still be acting in the fabric layers. In fact, under *p*-compression, the composite stiffness could be also represented on the basis of the contributions of the fabric layer (1) and interlayer material (2) according to the equation

$$E_{\parallel} = V_1 E_{1_{\parallel}} + V_2 E_{2_{\parallel}} \qquad (10)$$

$E_{2_{\parallel}}$ being particularly low when the composite materials are incompletely densified (weak interlayer bonding bridges), the composite stiffness under *p*-compression is roughly that of the fabric layer, i.e. that discussed in the previous section (see Fig. 14a):

$$E_{2_{\parallel}} \approx 0 \quad \text{and} \quad E_{\parallel} \approx V_1 E_{1_{\parallel}} \qquad (11)$$

On the other hand, under *o*-compression, the interlayer matrix can contribute to the composite compliance, as suggested in Fig. 15. Furthermore, the coupling between the fabric layer and the interlayer matrix can be now represented by the sum of the compliances rather than by that of the rigidities. Thus, the compliance of the composite can be given by

$$1/E_{\perp} = V_1/E_{\perp} + V_2/E_{2_{\perp}} \qquad (12)$$

Therefore, $E_{\perp}$ is not only depending on the fabric layer rigidity (as in *p*-direction) but appears to be mainly controlled by the interlayer rigidity. Since $E_{1_{\perp}} \gg E_{2_{\perp}}$, the composite compliance in the *o*-direction is given, in a first approximation, by $V_2/E_{2_{\perp}}$. This discussion leads to assume that when V_I is increased by dV_I during densification, a part of the compliant layers $V_2 dV_I$ is replaced by rigid layers so that

$$d(1/E_{\perp}) \sim V_2 dV_I (1/E_{1_{\perp}} - 1/E_{2_{\perp}}) \qquad (13)$$

since $E_{1_\perp} \gg E_{2_\perp}$ and, therefore, $E_\perp \approx E_{2_\perp}/V_2$, equation (13) leads to

$$d(1/E_\perp) \sim - dV_I/E_\perp \quad (14)$$

or

$$\frac{dE_\perp}{E_\perp} \sim dV_I \quad (15)$$

Thus, the variations of $E_\perp$ as a function of V_I appear to be exponential, at least in a first approximation, in agreement with the experimental data (see Fig. 4a and 5). It is noteworthy that the variations of $\sigma_\perp^R$ as a function of V_I (or $1 - V_p$ since $1 - V_p = V_C + V_I$ with V_C = constant) obey the same kind of exponential law (see Fig. 6a and 7).

Whatever the equations which are taken to describe the variations of $E_\parallel$ or $E_\perp$ as a function of V_I, the models which have been proposed result in a suitable fitting of the experimental data. They show that under both *o*- and *p*-compression in domain II, the variations of the stiffness of 2D-C–C/ceramic composites with V_I (or $1 - V_p$) follow either linear or non-linear laws which are all derived from rules of mixtures considering the materials as the association of bending elements or aggregates, or as that of compliant and rigid layers coupled in series or in parallel.

4.3. Damaging and rupture mechanisms

In domain III, 2D-C–C/ceramic composite materials exhibit a non-linear irreversible compression behaviour (Fig. 2). This domain is very wide under *o*-compression but rather limited under *p*-compression, particularly for highly densified materials. However, the damaging mechanisms which are involved must be considered with an equal attention for both *p*- and *o*-compression inasmuch as they give rise to energy dissipation that could result in rupture work improvements.

4.3.1. Failure mechanisms under o-compression

Under *o*-compression, 2D-C–C/ceramic composites have been already schematically described as a stacking of rigid and strong fibrous layers bound together by brittle matrix bridges [14, 15]. These ceramic bridges are the microstructural elements which break first when, under compression loading, the stress in each bridging ligament reaches the compression strength of the infiltrated ceramics. As the binding bridges fail, only part of their volume continues to contribute to the compression resistance, the other part remaining between the fabric layers as unloaded fragments.

If the ceramic binding bridges are assumed to be cylindrical (with a section s and a height a), the volume change related to their failure can be written as follows:

$$dv = a\,ds + s\,da \quad (16)$$

If one assumes that the volume of the degraded part of the ceramic binding bridges is proportional to the local deformation da, then

$$dv = ks\,da \quad (17)$$

where k is a constant.

Equations 16 and 17 lead to the following differential equation:

$$ds/s = (k - 1)da/a \quad \text{or} \quad ds/s = (k - 1)\varepsilon \quad (18)$$

where ε is the compression strain.

By integration, the relationship between the binding bridge cross section s and the compression strain ε is

$$s = s_0 \exp (k - 1)\varepsilon \quad (19)$$

where s_0 is the initial binding bridge cross section.

All along domain III, successive failures of the binding bridges take place when the stress in each binding bridge reaches the compression rupture strength of the infiltrated ceramics, i.e. when

$$\sigma_I^R = P/s \quad (20)$$

where P is the compression load applied to the binding bridges, which is also that applied on the bulk composite.

$$\sigma_\perp = P/S \quad (21)$$

where S is the apparent cross section of the composite sample.

Finally, by combining Equations 19, 20 and 21, a relationship between $\sigma_\perp$ and ε is derived:

$$\sigma_\perp = \sigma_\perp^0 \exp (k - 1)\varepsilon \quad \text{with} \quad \sigma_\perp^0 = s_0/s\,\sigma_I^R \quad (22)$$

As shown in Fig. 17, the experimental data are in good agreement with the exponential relationship (Equation 22). The $\sigma_\perp^0$ and k constants are given in Table V for 2D-C–C/TiC composites. This good agreement does confirm that the behaviour of such composites in *o*-compression is mainly depending on the interlayer material. In both the elastic and damaging domains (II and III respectively), the experimental data verify the model according to which the material is described as a stacking of rigid and strong layers (i.e. the coated fabric layers) and relatively weak layers (the interlayer C/ceramic hybrid matrix). As V_I (or $1 - V_p$) increases, the empty space between the binding bridges decreases, a feature which leads to invalidate the model in the upper part of domain III (see Fig. 2b). Thus, the exponential part of domain III is the more reduced as V_I (or $1 - V_p$) is high (Fig. 17). For highly densified materials, the extended upper part of domain III is thought to correspond to the progressive damaging by microcracking of the fabric layers themselves.

When, finally, the interlayer matrix is almost totally reduced to a powder, the fibres break resulting in composite failure (domain IV) (Fig. 2b).

4.3.2. Failure mechanisms under p-compression

The failure mechanisms of 2D-C–C/ceramic composites loaded in *p*-compression will be discussed on

TABLE V Experimental values of the constants of Equation 22 for 2D-C–C/TiC composite materials

V_{TiC}	$\sigma_\perp^0$ (MPa)	k
0	10	7.5
0.11	20	8.0
0.35	68	60

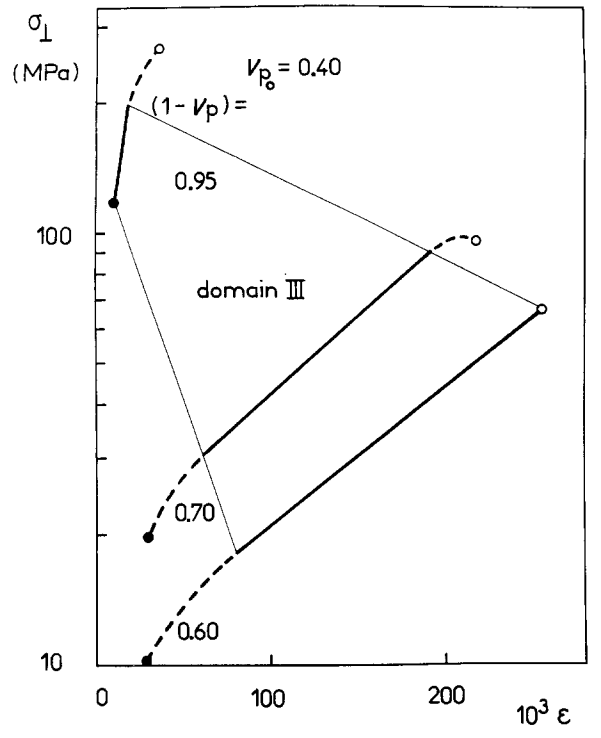

Figure 17 Stress-strain curves for 2D-C–C/ceramic composites loaded in *o*-compression (drawn in a semi-logarithmic scale). (○) ε^R, σ^R, (●) ε^D, σ^D.

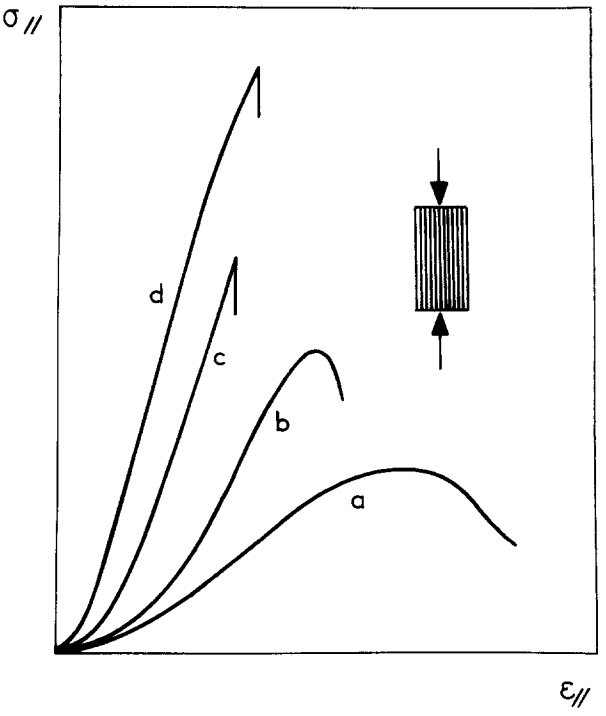

Figure 18 Main features of the stress–strain curves of 2D-C–C/ceramic composites loaded in *p*-compression.

the basis of (a) the rigidity of the infiltrated ceramic phase compared to that of the initial preform and (b) the thickness of the ceramic deposit, i.e. the degree of densification (or compacity).

4.3.2.1. Low degree of densification ($1 - V_p < 0.75$). In rather porous 2D-C–C/ceramic composites, microcracking occurs very early in the fibre ceramic coating (whose failure strain is quite small). The elastic energy released during this microcracking is not sufficient to break the fibres so that the fibrous layers are becoming more and more compliant as the load is increased. The weak interlayer bonding allows the fibrous layers to buckle up to a very significant value of strain. Then, the material fail by interlayer delamination. For composites corresponding to ceramics (e.g. BN or SiC + C) whose rigidities are close to that of pyrocarbon, the rupture strain tends to decrease when V_I (or $1 - V_p$) increases. Instability by buckling occurs indeed more and more readily (Fig. 18a).

On the other hand, composites slightly densified with very stiff ceramics (e.g. TiC, SiC or $\overline{B_4C}$) show a rupture strain which raises with increasing V_I. In such a case, the interlayer bonding strengthening due to the ceramics is sufficient enough to prevent an early buckling and allows fabric layer contraction under the applied *p*-compression load.

4.3.2.2. Medium degree of densification ($0.75 < 1 - V_p < 0.85$). For 2D-C–C/ceramic composites corresponding to a ceramic of low rigidity (e.g. BN), the matrix is still not stiff, or strong, enough to prevent fabric layer buckling and interlayer delamination. Thus, increasing V_I (or $1 - V_p$) does not change the failure mechanism but only raises the composite brittleness due to an increase in stiffness (Fig. 18b).

A similar increase in brittleness is observed for the materials corresponding to rigid ceramics such as TiC, SiC or $\overline{B_4C}$. Increasing V_I (or $1 - V_p$) raises the thickness of the brittle ceramic deposited on the fabric layers, giving rise to strong notch effects due to microcracks when, simultaneously, the elastic energy stored in the material and available for crack propagation is increased. As long as the interlayer bonding is not strong enough, the microcracks induce sudden fabric layer instabilities by buckling, leading to delamination prior to the failures of fibres and fabric layers (Fig. 18c).

4.3.2.3. Materials almost fully densified ($1 - V_p > 0.85$). No significant change in failure mechanism has been observed for the materials corresponding to weak matrices (e.g. BN) as full densification is approached. Rupture still occurs by delamination with an enhancement of the brittle character.

On the other hand, a transition from interlayer failure to intralayer failure, as compacity increases, systematically takes place in 2D-C–C/SiC and 2D-C–C/TiC composites. As densification proceeds towards completion, the interlayer, becoming more and more strong, impedes the propagation of the microcracks which have been initiated at the beginning of domain III. This increasing difficulty for the microcracks to propagate between the fabric layers is illustrated by the variations of the *p*-shear stress as a function of compacity (Fig. 19). Thus, in such highly densified composites, the microcracks propagate almost indifferently across or along fabric layers since the ceramic thickness which has to be fractured is nearly the same in any direction (2D-C–C/SiC or 2D-C–C/TiC composites are almost isotropic when approaching full densification). Moreover, the notch effect due to microcracks becomes so significant that fibres offer a

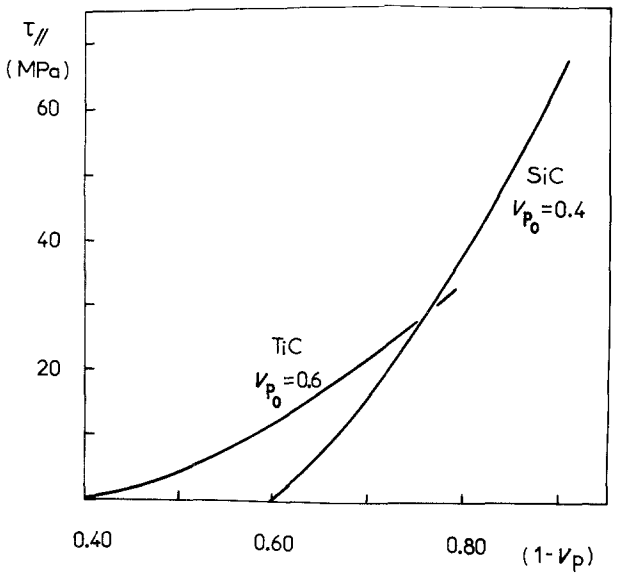

Figure 19 Variations of the *p*-shear stress as a function of compacity $1 - V_p$ for 2D-C–C/SiC and 2D-C–C/TiC composites. τ = shear stress.

poor resistance to crack propagation. As a result, the rupture surface is macroscopically orientated at about 45° with respect to loading direction i.e. in the plane where the shear stress is maximum (Fig. 20b). The occurrence of a transition in the failure mode is of significant interest since it suggests that failure mechanism could be controlled and rupture work increased by optimizing the material microstructure (i.e. the fibre–matrix interfaces or the matrix–matrix interfaces in order to enhance their impeding effect on microcrack propagation). More generally speaking, the aim of such microstructure optimization should be to generate within the composite material numerous possible ways for microcrack propagation in order to increase the rupture surface giving rise to larger energy dissipation (Fig. 18d). It is noteworthy that the transition in failure mode corresponds actually to an increase in rupture strain, as shown in Fig. 8 for 2D-C–C/TiC composites.

Such a transition has not been observed yet for the related 2D-C–C/$\overline{B_4C}$ composites due possibly to (i) a larger elastic energy release during microcracking of the $\overline{B_4C}$ matrix resulting in a higher crack growth rate and/or (ii) an insufficient $\overline{B_4C}$ volume fraction. This last consideration could result from an inhomogeneous densification that had lead to an overestimation of the actual compacity ($1 - V_p$ values were derived from weight increase). This argument would explain the anomalies observed for 2D-C–C/$\overline{B_4C}$ composites referred to as "fully densified" (see Fig. 5 (dashed line) and Table II (δ value)). Therefore, we consider that the damaging mechanism, corresponding to a 45° failure mode, is also applicable to 2D-C–C/$\overline{B_{44}C}$ composites actually completely densified.

5. Summary

2D-C–C/ceramic composite materials have been investigated from the stand-point of their mechanical response to compression loading in directions parallel or perpendicular to the fabric layers. Three types of behaviour have been observed: (i) a non-linear and time dependent behaviour for weakly densified materials, (ii) a quasi-linear elastic domain which is quite extended under *p*-compression, (iii) a "pseudo-plastic" character

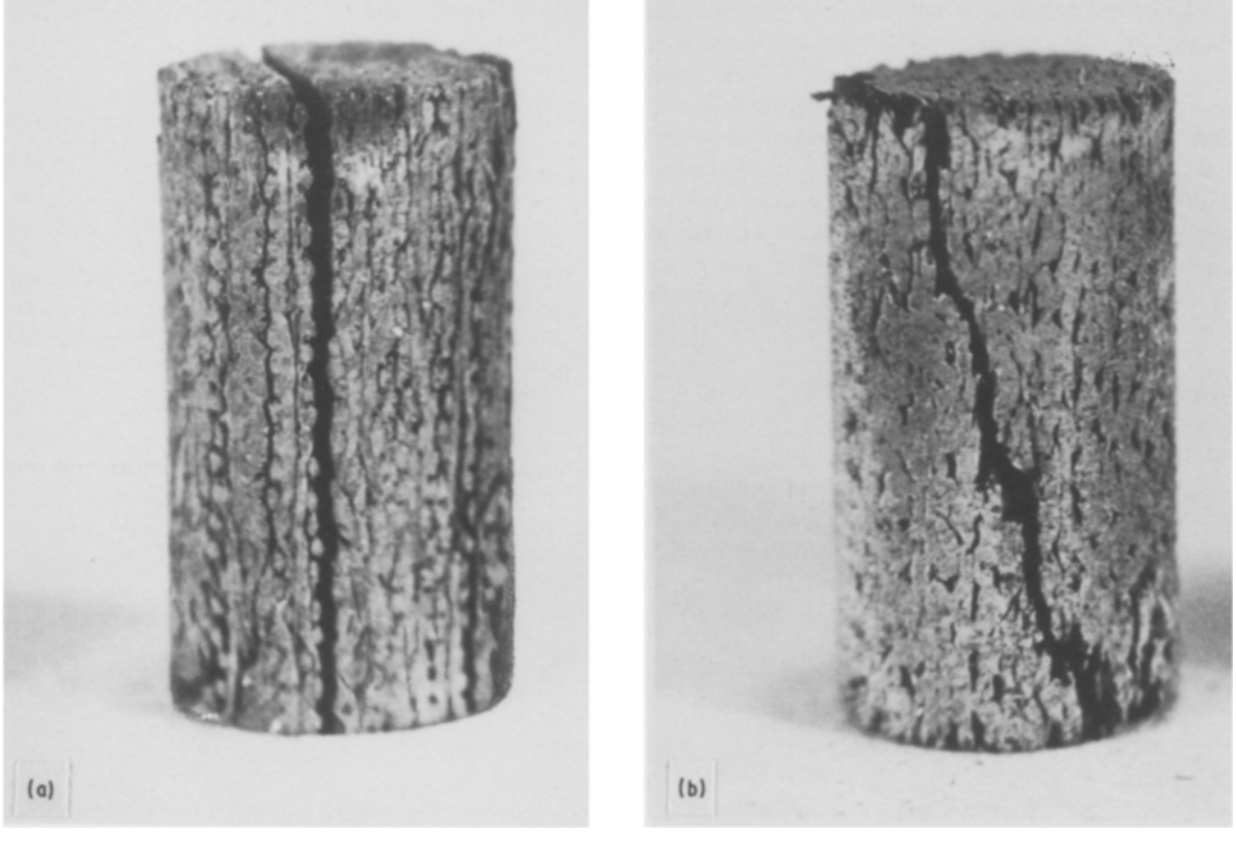

Figure 20 Failure modes of 2D-C–C/ceramic composites loaded in *p*-compression (a) low densification state, (b) full densification state.

corresponding to various damaging mechanisms leading to energy dissipation. Although the time-dependency of the mechanical behaviour is apparently not very significant for fully densified materials, it is indicative of damping effects which suggest to pay attention to load cycling behaviours.

Regarding the elastic moduli derived from the stress–strain curves, it comes out that the general addition (or mixture) laws depict quite well the mechanical behaviours of 2D-C–C/ceramic composites provided the following models are accepted: (i) under *p*-compression, poorly densified composites behave as the association in parallel of fabric layers whose contraction is due to the bending of numerous elementary microstructural beams. The composite rigidity is proportional to those of the elementary beams (i.e. $E_{\parallel} \sim E_C V_C^2 + E_I V_I^2 + 2E_I V_I V_C$), (ii) under *p*-compression, fully densified composites can be represented by the coupling in parallel of compliances corresponding to carbon, the infiltrated ceramic (and pores). Thus, the composite rigidity is given by the usual rule of mixture (i.e. $E_{\parallel} \approx E_C V_C + E_I V_I$), (iii) under *o*-compression, the composites can be considered as a stacking of alternating rigid fabric layers and compliant matrix interlayers. In such a coupling in series, the composite compliance is given again by a mixture law (i.e. $1/E_{\perp} \approx V_1/E_{1_{\perp}} + V_2/E_{2_{\perp}}$).

On the basis of the above models, the variations of the composite rigidity as a function of compacity can be predicted. It is respectively parabolic or linear in the first and second models (*p*-compression) and exponential in the third (*o*-compression). It is noteworthy that very similar laws were found for compression rupture strength.

Under *o*-compression, failure occurs as the result of damaging mechanisms which tend to degrade the ceramic bridges binding together the fabric layers. Under *p*-compression, a transition in failure mode takes place as compacity reaches a critical value of about 0.85 provided the infiltrated ceramic is strong enough. Delamination (the most common failure mode) is replaced by intralayer failure, giving rise to energy dissipation. The occurrence of such a transition in failure mode suggests several microstructural possibilities to improve the toughness of 2D-C–C/ceramic composite materials.

Acknowledgements

The authors wish to thank R. Pailler, Y. Le Petitcorps and J. M. Birbis for their advice as well as Société Européenne de Propulsion for the supply of the 2D-C–C preforms and technical assistance in some of the mechanical tests. This work has been partly supported by the French Ministries of Defense (DRET) and Research and Technology (MRT).

References

1. F. CHRISTIN, R. NASLAIN and C. BERNARD, in Proceedings CVD-VII, edited by T. O. Sedwick and H. Lydtin (The Electrochemical Society, Princeton, 1979) p. 499.
2. C. MALLET, R. NASLAIN, J. THEBAULT and B. BUTTAZZONI, International Symposium on Carbon Toyohashi, Ext. Abstracts, Suppl. 1002, pp. 1-4, Kagahu Gijutsu-ha, Tokyo, 1982.
3. J. Y. ROSSIGNOL, R. NASLAIN, P. HAGENMULLER, L. HERAUD and J. J. CHOURY,in Proceedings Euro CVD-III, edited by H. E. Hintermann (LSRH, Neuchâtel, 1980) p. 162.
4. H. HANNACHE, J. Y. ROSSIGNOL, F. LANGLAIS, R. NASLAIN and P. HAGENMULLER, *J. Less-common Metals* (in press).
5. H. HANNACHE, R. NASLAIN and C. BERNARD, *ibid.* **95** (1983) 221.
6. J. Y. ROSSIGNOL, F. LANGLAIS and R. NASLAIN, in Proceedings CVD-IX, Cincinnati, edited by Mc D. Robinson (The Electrochem. Soc., Pennington, 1984) p. 596.
7. R. NASLAIN and F. LANGLAIS, in "Tailoring Multiphase and Composite Ceramics," edited by R. T. Tessler, G. L. Messing, C. G. Pantano and R. E. Newnham (Materials Science Research, Plenum Press, New York, 1986) p. 145.
8. R. NASLAIN, J. Y. ROSSIGNOL, P. HAGENMULLER, F. CHRISTIN, L. HERAUD and J. J. CHOURY, *Rev. Chimie Minérale*, **18** (1981) 544.
9. C. MALLET, PhD thesis No. 1811, University of Bordeaux, France (1982).
10. H. HANNACHE, PhD thesis No. 813, University of Bordeaux, France (1984).
11. R. NASLAIN, P. HAGENMULLER, F. CHRISTIN, L. HERAUD and J. J. CHOURY, in "Advances in Composite Materials"/ICCM-3 vol. 2, edited by A. R. Bunsell, C. Bathias, A. Hartreucher, D. Menties and G. Verchery (Pergamon Press, Paris, 1980) p. 1084.
12. J. Y. ROSSIGNOL, R. NASLAIN, P. HAGENMULLER and L. HERAUD, in "Progress in Science and Engineering of Composites/ICCM-IV" edited by T. Hayashi (Tokyo, 1982) p. 1227
13. H. HANNACHE, J. M. QUENISSET, R. NASLAIN and L. HERAUD, *J. Mater. Sci.*, **19** (1984) 202.
14. J. Y. ROSSIGNOL, J. M. QUENISSET and R. NASLAIN, *Composites* **18**(2) (1987) 135.
15. R. NASLAIN, J. M. QUENISSET, J. Y. ROSSIGNOL, H. HANNACHE, P. LAMICQ, J. J. CHOURY, L. HERAUD and F. CHRISTIN, in Proceedings ICCM-V, San Diego edited by W. C. Harrigan (TMS-AIME, Warrendale, Pennsylvania, 1985) p. 499.
16. M. DAUCHIER, G. BERNHART and C. BONNET, in Proceedings 30th National SAMPE, Anaheim, 30 (Covina, California, 1985) 1519–1525.
17. P. J. LAMICQ, G. A. BERNHART, M. M. DAUCHIER and J. G. MACÉ, *Amer. Ceram. Bull.* **65**/2 (1986) 336.
18. A. J. CAPUTO, R. A. LOWDEN and D. P. STINTON, ORNL/TR-9651, NTIS, US Dep. Commerce, Springfield, Virginia (1985)
19. E. FITZER and R. GADOW, *Amer. Ceram. Bull.*, **65**/2 (1986) 326.

Received 13 October 1986
and accepted 22 January 1987